SUPPLEMENTARY INFORMATION

Tuning the electronic structure of thiolate-protected 25-atom clusters by co-substitution with metals having different preferential sites

Sachil Sharma,[a] Seiji Yamazoe,[b,c] Tasuku Ono,[a] Wataru Kurashige,[a] Yoshiki Niihori,[a] Katsuyuki Nobusada,[c,d,*] Tatsuya Tsukuda,[b,c,*] and Yuichi Negishi[a,e,*]

[a] *Department of Applied Chemistry, Faculty of Science, Tokyo University of Science, 1-3 Kagurazaka, Shinjuku-ku, Tokyo 162−8601, Japan.*
[b] *Department of Chemistry, Faculty of Science, University of Tokyo, 7−3−1 Hongo, Bunkyo−ku, Tokyo 113−0033, Japan.*
[c] *Elements Strategy Initiative for Catalysts and Batteries (ESICB), Kyoto University, Katsura, Kyoto 615−8520, Japan.*
[d] *Department of Theoretical and Computational Molecular Science, Institute for Molecular Science, Myodaiji, Okazaki, Aichi 444−8585, Japan.*
[e] *Photocatalysis International Research Center, Tokyo University of Science, 2641 Yamazaki, Noda, Chiba 278−8510, Japan.*

Corresponding Author E-mail:
negishi@rs.kagu.tus.ac.jp (Y. N.)
tsukuda@chem.s.u-tokyo.ac.jp (T. T.)
nobusada@ims.ac.jp (K. N.)

1. Experimental Procedures

1.1. Chemicals

All chemicals were commercially obtained and used without further purification. Hydrogen tetrachloroaurate tetrahydrate ($HAuCl_4 \cdot 4H_2O$) was purchased from Tanaka Kikinzoku. Palladium(II) sodium chloride trihydrate ($PdCl_2 \cdot 2NaCl \cdot 3H_2O$), silver nitrate ($AgNO_3$), copper(II) chloride dihydrate ($CuCl_2 \cdot 2H_2O$), tetraoctylammonium bromide ($(C_8H_{17})_4NBr$), sodium tetrahydroborate ($NaBH_4$), 1-dodecanethiol ($C_{12}H_{25}SH$), triethylamine, and dichloromethane (CH_2Cl_2) were obtained from Wako Pure Chemical Industries. Methanol, ethanol, toluene, and acetone were obtained from Kanto Kagaku. Tetrabutylammonium perchlorate ($(C_4H_9)_4NClO_4$) and *trans*-2-[3-(4-*tert*-butylphenyl)-2-methyl-2-propenylidene]malononitrile (DCTB) were purchased from Tokyo Kasei. Deionized water with a resistivity of > 18 MΩ cm was used in all experiments.

1.2. Synthesis

1.2.1 $Au_{24}Pd(SC_{12}H_{25})_{18}$ template cluster

This synthesis includes four steps: (1) the synthesis of a mixture of $[Au_{24}Pd(SC_{12}H_{25})_{18}]^{2-/-/0}$ and $[Au_{25}(SC_{12}H_{25})_{18}]^-$,[1] (2) the oxidation of part of the samples to the neutral form, (3) the rough separation of neutral $Au_{24}Pd(SC_{12}H_{25})_{18}$ from $Au_{25}(SC_{12}H_{25})_{18}$ by solvent extraction, and (4) the complete removal of $Au_{25}(SC_{12}H_{25})_{18}$ from the sample by thiol etching. Specifically, a mixture of $[Au_{24}Pd(SC_{12}H_{25})_{18}]^{2-/-/0}$ and $[Au_{25}(SC_{12}H_{25})_{18}]^-$ were firstly prepared according to our previous report with slight modification.[1] The mixture (~50 mg) was kept in CH_2Cl_2 (100 mL) containing $(C_4H_9)_4NClO_4$ (342 mg) at room temperature for ~3.5 h. It is presumed that under these conditions, most of the $[Au_{24}Pd(SC_{12}H_{25})_{18}]^{2-/-}$ clusters are oxidized to the neutral form, whereas most of the $[Au_{25}(SC_{12}H_{25})_{18}]^-$ ones are not. Then, anionic $[Au_{25}(SC_{12}H_{25})_{18}]^-$ was removed from the sample by solvent extraction using acetone. The resulting sample still contained a small amount of $Au_{25}(SC_{12}H_{25})_{18}$, as confirmed by matrix-assisted laser desorption ionization (MALDI) mass spectrometry of the sample. The sample (~6 mg) was dissolved in toluene/acetone (2:1; 30 mL) containing dodecanethiol (2 mL) and stirred at room temperature for 2 days. This etching process was repeated until $Au_{25}(SC_{12}H_{25})_{18}$ was completely removed from the sample. The obtained product was further purified using a size exclusion

column (Waters Co., Ultrastyragel^{TM}) to remove the by-product produced during the etching procedure. The final product was highly pure, as shown in the upper part of Fig. 2(a).

1.2.2 M-dodecanethiol complex (M = Ag or Cu)

Metal-$SC_{12}H_{25}$ complexes were synthesized by a method similar to that reported for synthesis of a metal-SC_2H_4Ph complex.[2] First, $AgNO_3$ (770 mg) or $CuCl_2 \cdot 2H_2O$ (607 mg) was dissolved in a small amount of water and then ethanol (5 mL) was added. Each mixture was vigorously stirred until the metal salts fully dissolved. Separately, $C_{12}H_{25}SH$ (1.09 mL) was dissolved in a mixture of ethanol (7 mL) and trimethylamine (2 mL). This solution was added to each metal salt solution. After vigorous stirring for 30 min, the reaction solution was centrifuged. The resulting precipitates were washed several times with a mixture of water and ethanol (1:1) and subsequently with a pure ethanol.

1.2.3 $Au_{24-x}Ag_xPd(SC_{12}H_{25})_{18}$ trimetallic cluster

This cluster was prepared using a reported metal exchange method.[2,3] Pure $Au_{24}Pd(SC_{12}H_{25})_{18}$ (5 mg) was dissolved in toluene (5 mL) and then Ag-$SC_{12}H_{25}$ (10 mg) was added. The solution was stirred at room temperature. Aliquots of the reaction solution (~150 µL) were taken out at regular time intervals and centrifuged to remove the by-products and unreacted Ag-$SC_{12}H_{25}$. The supernatant was evaporated to dryness and the residue was washed with methanol three times. The resulting product was characterized by MALDI mass spectrometry (Fig. 2(a)) and UV-Vis spectroscopy (Fig. 4(a)). The number of Ag atoms included in the cluster increased with the quantity of the reacted Ag-SC12 complex. For example, we observed the inclusion of Ag atoms up to 7 when the quantity of Ag-SC12 was increased up to 15 mg.

1.2.4 $Au_{24-y}Cu_yPd(SC_{12}H_{25})_{18}$ trimetallic cluster

This cluster was also prepared using the metal exchange method.[2,3] Specifically, $Au_{24}Pd(SC_{12}H_{25})_{18}$ (4 mg) was dissolved in toluene (4 mL) and then Cu-$SC_{12}H_{25}$ (4 mg) was added. In this synthesis, $NaBH_4$ (2 mg) was also added to the reaction medium, similar to the reaction between $Au_{25}(SC_2H_4Ph)_{18}$ and Cu-SC_2H_4Ph.[2] Aliquots of the reaction solution (~150 µL) were taken out after regular time intervals and centrifuged to remove the by-products and unreacted Cu-$SC_{12}H_{25}$. The supernatant was evaporated to dryness and the residue was washed with methanol three times. The resulting product was characterized by MALDI mass spectrometry (upper spectrum of Fig. S6).

1.2.5 $Au_{24-x-y}Ag_xCu_yPd(SC_{12}H_{25})_{18}$ tetrametallic cluster

This cluster was prepared from $Au_{24-x}Ag_xPd(SC_{12}H_{25})_{18}$ and Cu-$SC_{12}H_{25}$ or $Au_{24-y}Cu_yPd(SC_{12}H_{25})_{18}$ and Ag-$SC_{12}H_{25}$ using the metal exchange method.[2,3] In the former preparation, $Au_{24-x}Ag_xPd(SC_{12}H_{25})_{18}$ (2 mg) was dissolved in toluene (2 mL) and then Cu-$SC_{12}H_{25}$ (2 mg) was added. In the latter preparation, $Au_{24-y}Cu_yPd(SC_{12}H_{25})_{18}$ (2 mg) was dissolved in toluene (2 mL) and then Ag-$SC_{12}H_{25}$ (2 mg) was added. The solutions were both stirred at room temperature. Aliquots of the reaction solutions (~150 µL) were taken out at regular time intervals and centrifuged to remove the by-products and unreacted M-$SC_{12}H_{25}$ (M = Ag or Cu). Each supernatant was evaporated to dryness and then washed with methanol three times. The resulting products were characterized by MALDI mass spectrometry (Fig. 2(b), S5 and S6) and UV-Vis spectroscopy (Fig. 4(b)).

1.3. Characterization

MALDI mass spectra were acquired using a spiral time-of-flight mass spectrometer (JEOL Ltd., JMS-S3000) with a semiconductor laser (wavelength: 349 nm). DCTB was used as the matrix.[4] The cluster-to-matrix ratio was set to 1:1000.

Pd K-edge, Ag K-edge and Cu K-edge X-ray absorption fine structure (XAFS) measurements were carried out at the BL01B1 beamline at the SPring-8 facility of the Japan Synchrotron Radiation Research Institute (proposal nos. 2015A1590, 2015B1308, and 2016A1436). Measurements were conducted at 10 K.[5] A Si (311) two-crystal monochromator was used as the incident beam. $Au_{24}Pd(SC_{12}H_{25})_{18}$, $Au_{24-x}Ag_xPd(SC_{12}H_{25})_{18}$, and $Au_{24-x-y}Ag_xCu_yPd(SC_{12}H_{25})_{18}$ diluted with boron nitride were pressed into a pellet and mounted on a sample holder attached to the cryostat. Subsequently, Pd, Ag and Cu K-edge XAFS spectra were recorded in fluorescence mode using an ionization chamber as the I_0 detector and 19 solid state detectors as the I detector. The X-ray energy was calibrated using Pd, Ag and Cu foils for Pd, Ag and Cu K-edge data, respectively. Data analysis was performed with the REX2000 Ver. 2.5.9 software package (Rigaku). The extended X-ray absorption fine structure (EXAFS) data for the Pd, Ag, and Cu K-edge were analyzed as follows. The χ spectra were extracted by removing the atomic absorption background using a cubic spline and were normalized to the edge height. The k^3-weighted χ spectra underwent a Fourier transform (FT) into r space using a k range of 3.0–15.5 $Å^{-1}$ for the Pd K-edge, 3.0–14.0 $Å^{-1}$ for the Ag K-edge, and 3.0–11.0 $Å^{-1}$ for the Cu K-edge. The curve fitting ranges of Pd–M (M = Au and/or Ag), Ag–M (M = Au and/or Pd), and Ag–S, Cu–S were 1.9–3.0, 1.7–3.1, 1.4–2.3 Å, respectively. The phase shift and backscattering amplitude functions of Pd–Au, Pd–Ag, Ag–Au, Ag–S, and Cu–S bonds were extracted from $PdAgAu_{23}(SCH_3)_{18}$ (Pd: center, Ag: edge), $AgAu_{24}(SCH_3)_{18}$ (Ag: edge), and $CuAu_{24}(SCH_3)_{18}$ (Cu: staple) using FEFF8 (σ^2 = 0.0036, where σ is the Debye–Waller factor).

Diffuse reflectance spectra of the samples were acquired at ambient temperature using a JASCO V-670 spectrometer. The wavelength-dependent optical data, I(w), were converted to energy-dependent data, $I(E)$, using the following equation, which conserves the integrated spectral areas:

$I(E) = I(w)/|\partial E/\partial w| \propto I(w) \times w^2$.

2. Calculations

Density functional theory (DFT) calculations were performed for $[Au_{24}Pd(SCH_3)_{18}]^0$,[1] $[Au_{23}AgPd(SCH_3)_{18}]^0$ (Fig. 5(a)), and $[Au_{22}AgCuPd(SCH_3)_{18}]^0$ (Fig. 5(a) and S12). In these calculations, the experimentally synthesized clusters were modeled by replacing dodecanethiolate with methanethiolate. Geometric optimizations of $[Au_{23}AgPd(SCH_3)_{18}]^0$ and $[Au_{22}AgCuPd(SCH_3)_{18}]^0$ were performed starting from an initial structure estimate based on $[Au_{24}Pd(SCH_3)_{18}]^0$ (ref. 1). This initial structure appears to be relatively symmetric. However, we did not assume a high degree of molecular symmetry in our calculations and instead performed full geometry optimization of each cluster. The TURBOMOLE package of *ab initio* quantum chemistry programs[6] was used in all calculations. Geometric optimizations based on a quasi-Newton–Raphson method were performed at the level of Kohn-Sham (KS) DFT using the Becke three-parameter hybrid exchange functional with the Lee–Yang–Parr correlation functional (B3LYP).[7,8] The double-ζ valence quality plus polarization basis in the TURBOMOLE basis set library was used in the calculations, along with a 60-electron (28-electron) relativistic effective core potential[9] for the gold (palladium or silver) atoms. Optimized structures of these clusters with different substitution positions, and the -S(R)-[Au-S(R)-]$_2$ staple were obtained at the same level of theory. The absorption spectra were simulated using time-dependent KS linear response theory.[10–12]

3. Results

Table S1. Trimetallic $Au_{24-x}Ag_xPd(SC_{12}H_{25})_{18}$ and Tetrametallic $Au_{24-x-y}Ag_xCu_yPd(SC_{12}H_{25})_{18}$ having Similar Molecular Weights.

Chemical Formula	Molecular weight (Da) [a]
$Au_{21}Ag_3Pd(SC_{12}H_{25})_{18}$	8191.4
$Au_{22}Cu_2Pd(SC_{12}H_{25})_{18}$	8191.9
$Au_{20}Ag_4Pd(SC_{12}H_{25})_{18}$	8102.3
$Au_{21}AgCu_2Pd(SC_{12}H_{25})_{18}$	8102.8
$Au_{20}Ag_2CuPd(SC_{12}H_{25})_{18}$	8058.0
$Au_{21}Cu_3Pd(SC_{12}H_{25})_{18}$	8058.4
$Au_{19}Ag_5Pd(SC_{12}H_{25})_{18}$	8013.2
$Au_{20}Ag_2Cu_2Pd(SC_{12}H_{25})_{18}$	8013.7
$Au_{19}Ag_4CuPd(SC_{12}H_{25})_{18}$	7968.9
$Au_{20}AgCu_3Pd(SC_{12}H_{25})_{18}$	7969.3

[a]These values were calculated using "Isotope Pattern Simulator" software.

Table S2. Results of Curve Fitting Analysis of Pd K-edge EXAFS Data for $Au_{24}Pd(SC_{12}H_{25})_{18}$, $Au_{24-x}Ag_xPd(SC_{12}H_{25})_{18}$, and $Au_{24-x-y}Ag_xCu_yPd(SC_{12}H_{25})_{18}$.

Cluster	Bond	C.N. [a,b]	r (Å) [a]	D.W. [a,c]	R factor (%) [a]
$Au_{24}Pd$	Pd–Au	11.0(1.0)	2.769(2)	0.0058(8)	14.2
$Au_{24-x}Ag_xPd$	Pd–Ag	1.8(1.6)	2.782(24)	0.002(16)	6.7
	Pd–Au	8.5(1.7)	2.726(8)	0.005(3)	
$Au_{24-x-y}Ag_xCu_yPd$	Pd–Ag	1.0(3)	2.724(15)	0.005(1)	10.3
	Pd–Au	10.8(1.8)	2.755(9)	0.005(12)	

Numbers in parentheses are uncertainties; 2.769(2) represents 2.769 ± 0.002.
[a]The values were obtained by fitting with Pd–Au and Pd–Ag bonds.
[b]Coordination number.
[c]$\Delta DW = \{(\sigma-\sigma_0)^2\}$, where σ and σ_0 represent Debye–Waller factors of the sample and standard value (0.06), respectively.

Table S3. Results of Curve Fitting Analysis of Ag K-edge EXAFS Data for $Au_{24-x}Ag_xPd(SC_{12}H_{25})_{18}$ and $Au_{24-x-y}Ag_xCu_yPd(SC_{12}H_{25})_{18}$.

Cluster	Bond	C.N. [a,b]	r (Å) [a]	D.W. [a,c]	R factor (%) [a]
$Au_{24-x}Ag_xPd$	Ag–S	1.4(4)	2.487(10)	0.011(5)	11.5
	Ag–Pd	0.9(3)	2.786(6)	0.006(3)	
	Ag–Au	4.5(9)	2.850(17)	0.017(3)	
$Au_{24-x-y}Ag_xCu_yPd$	Ag–S	1.1(3)	2.460(10)	0.009(6)	14.3
	Ag–Pd	1.2(6)	2.754(14)	0.013(10)	
	Ag–Au	4.5(12)	2.863(13)	0.015(5)	

Numbers in parentheses are uncertainties; 2.485(13) represents 2.485 ± 0.013.
[a]The values were obtained by fitting with Ag–S, Ag–Pd and Ag–Au bonds.
[b]Coordination number.
[c]$\Delta DW = \{(\sigma-\sigma_0)^2\}$, where σ and σ_0 represent the Debye–Waller factor of the sample and standard value (0.06), respectively.

Table S4. Results of Curve Fitting Analysis of Cu K-edge EXAFS Data for $Au_{24-x-y}Ag_xCu_yPd(SC_{12}H_{25})_{18}$.

Cluster	Bond	C.N. [a,b]	r (Å) [a]	D.W. [a,c]	R factor (%) [a]
$Au_{24-x-y}Ag_xCu_yPd$	Cu–S	2.2(3)	2.280(4)	0.012(2)	14.8

Numbers in parentheses are uncertainties; 2.251(9) represents 2.251 ± 0.009.
[a]The values were obtained by fitting with Cu–S bonds.
[b]Coordination number.
[c]$\Delta DW = \{(\sigma-\sigma_0)^2\}$, where σ and σ_0 terms represent Debye–Waller factors of the sample and standard value (0.06).

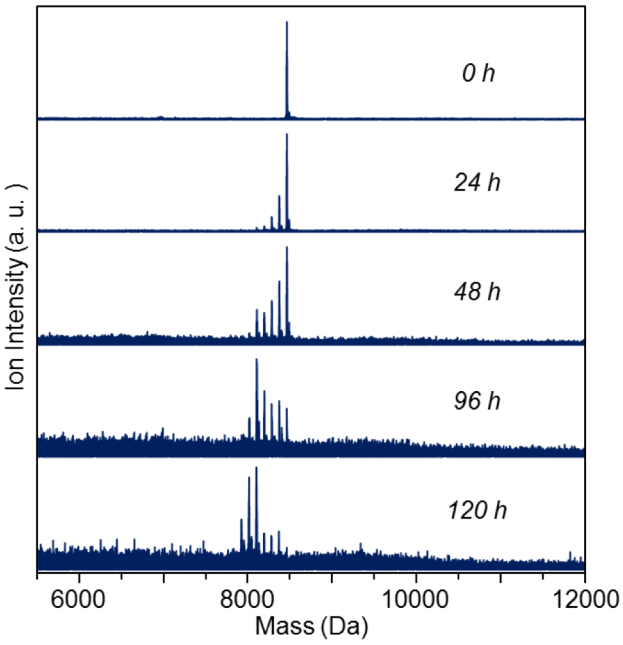

Fig. S1 Wide region of the negative-ion MALDI mass spectra of the clusters before and after the reaction between $Au_{24}Pd(SC_{12}H_{25})_{18}$ and Ag-$SC_{12}H_{25}$. These mass spectra demonstrate that each sample does not include clusters of other sizes in a similar size region.

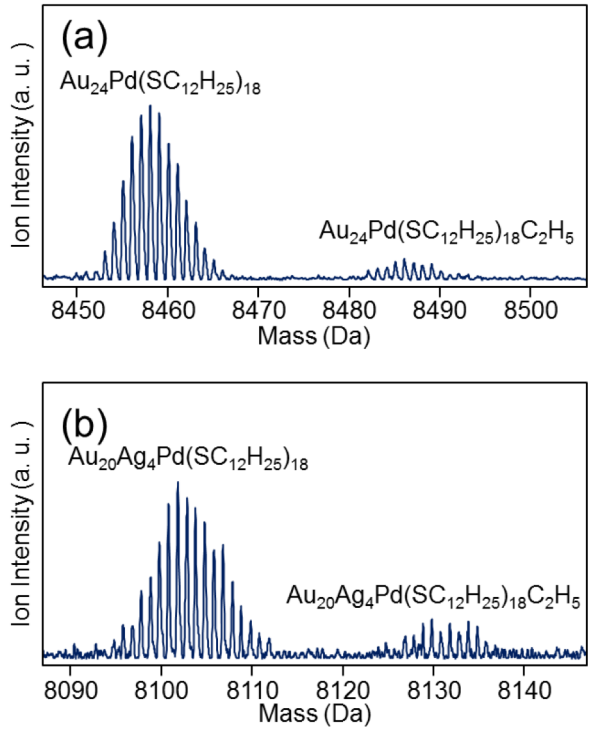

Fig. S2 Assignments of the sub-peaks appearing just on the right of (a) the bimetallic and (b) the trimetallic clusters. These peaks probably originate from the C_2H_5 radical adduct. This type of adduct peak has sometimes been observed in MALDI mass spectra.[13–15] In this study, these peaks did not disappear even when the laser fluence was decreased to the lowest value that enabled us to detect the ions.

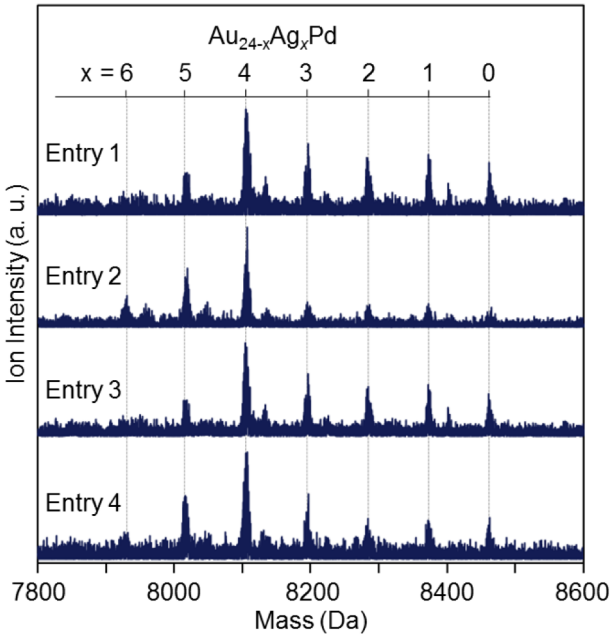

Fig. S3 Negative-ion MALDI mass spectra of the products after reaction of $Au_{24}Pd(SC_{12}H_{25})_{18}$ with Ag-$SC_{12}H_{25}$ for a long time. The peak attributed to $Au_{20}Ag_4Pd(SC_{12}H_{25})_{18}$ was always observed with the highest ion intensity in the mass spectra, meaning that $Au_{20}Ag_4Pd(SC_{12}H_{25})_{18}$ is the most stable cluster among $Au_{24-x}Ag_xPd(SC_{12}H_{25})_{18}$ clusters under the investigated experimental conditions.

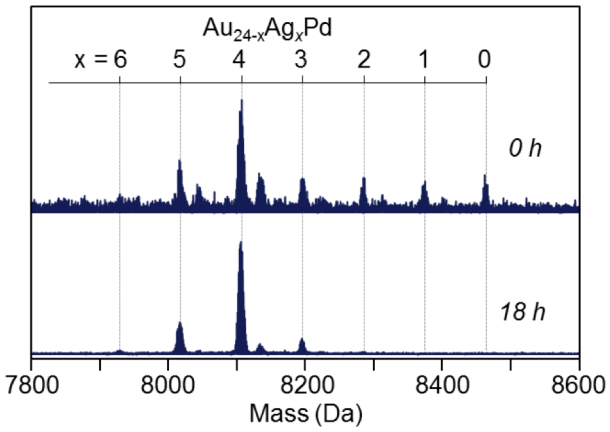

Fig. S4 Result of the stability experiments. In this experiments, $Au_{24-x}Ag_xPd(SC_{12}H_{25})_{18}$ clusters were left in toluene (1.5 mL) containing $C_{12}H_{25}SH$ (1.5 mL) at 50 °C.

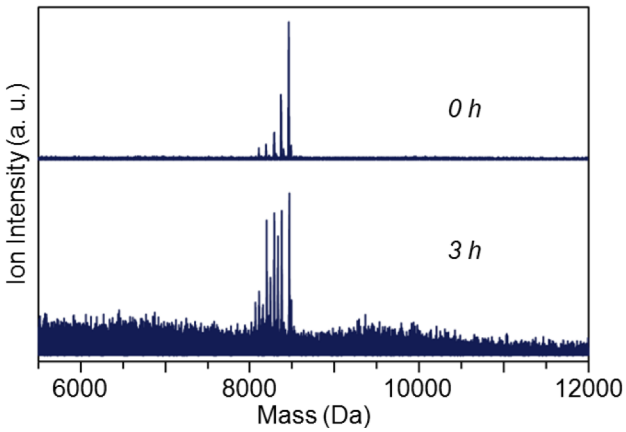

Fig. S5 Wide region of the negative-ion MALDI mass spectra of the clusters before and after the reaction between $Au_{24-x}Ag_xPd(SC_{12}H_{25})_{18}$ and Cu-$SC_{12}H_{25}$. These mass spectra demonstrate that each sample does not include clusters of other sizes in a similar size region.

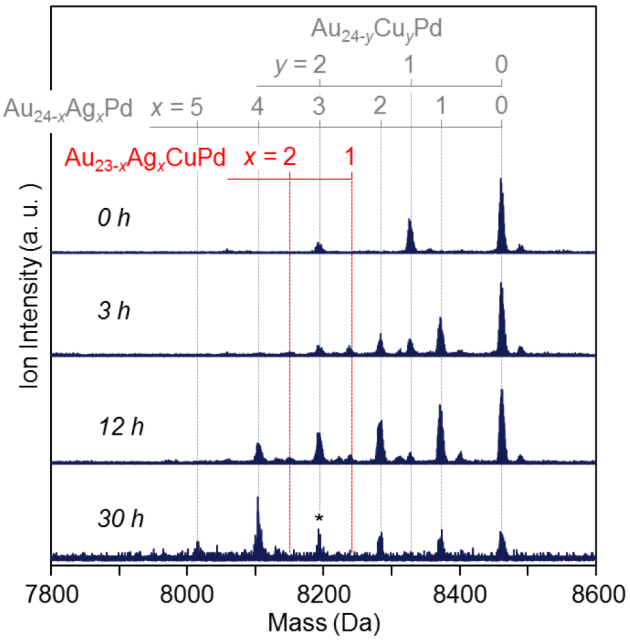

Fig. S6 Negative-ion MALDI mass spectra of the products obtained by the reaction between $Au_{24-y}Cu_yPd(SC_{12}H_{25})_{18}$ and Ag-$SC_{12}H_{25}$. The peaks with asterisks could include two species (Table S1).

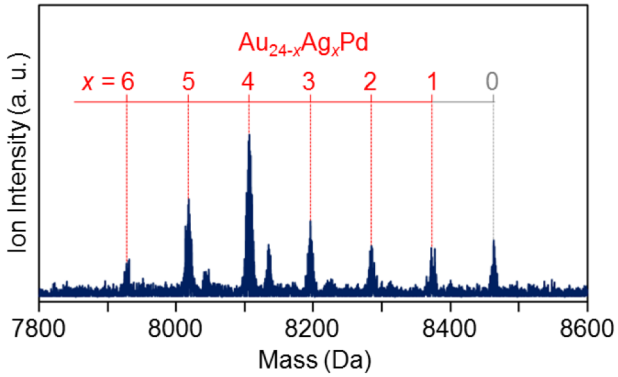

Fig. S7 Negative-ion MALDI mass spectra of the product used for the EXAFS experiments of trimetallic $Au_{24-x}Ag_xPd(SC_{12}H_{25})_{18}$. Because the sample was prepared in a short reaction time to obtain information on the initial substitution site of Ag, bimetallic $Au_{24}Pd(SC_{12}H_{25})_{18}$ is also observed in this sample. The estimation of the peak area ratio in the mass spectra suggests that in this sample, 91.5 % of Pd atoms are included in trimetallic $Au_{24-x}Ag_xPd(SC_{12}H_{25})_{18}$ ($x \neq 0$). This means that the spectral feature in the Pd K-edge FT-EXAFS spectrum of this sample (Fig. 3(a)) is governed by Pd in trimetallic $Au_{24-x}Ag_xPd(SC_{12}H_{25})_{18}$ ($x \neq 0$). Regarding Ag, all the Ag atoms in this sample are present in trimetallic $Au_{24-x}Ag_xPd(SC_{12}H_{25})_{18}$ ($x \neq 0$). Thus, the spectral feature in the Ag K-edge FT-EXAFS spectrum of this sample (Fig. 3(b)) shows the Ag substitution site in trimetallic $Au_{24-x}Ag_xPd(SC_{12}H_{25})_{18}$ ($x \neq 0$).

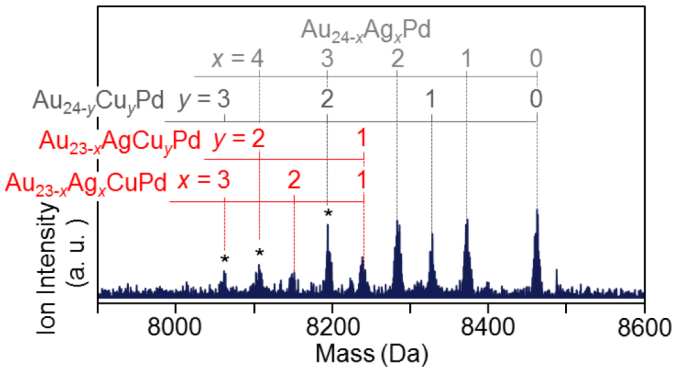

Fig. S8 Negative-ion MALDI mass spectra of the product used for the EXAFS experiments of tetrametallic $Au_{24-x-y}Ag_xCu_yPd(SC_{12}H_{25})_{18}$. In this sample, the trimetallic $Au_{24-x}Ag_xPd(SC_{12}H_{25})_{18}$ and $Au_{24-y}Cu_yPd(SC_{12}H_{25})_{18}$ are also present, because the sample was prepared in a short reaction time to obtain information on the initial substitution sites of Ag and Cu. The peaks with asterisks could include two species (Table S1). It was estimated that in this sample, 30.0% of Pd atoms, 43.1% of Ag atoms, and 46.5% of Cu atoms are present in tetrametallic $Au_{24-x-y}Ag_xCu_yPd(SC_{12}H_{25})_{18}$ ($x \neq 0$, $y \neq 0$) under the assumption that those peaks include two species with the same ratio.

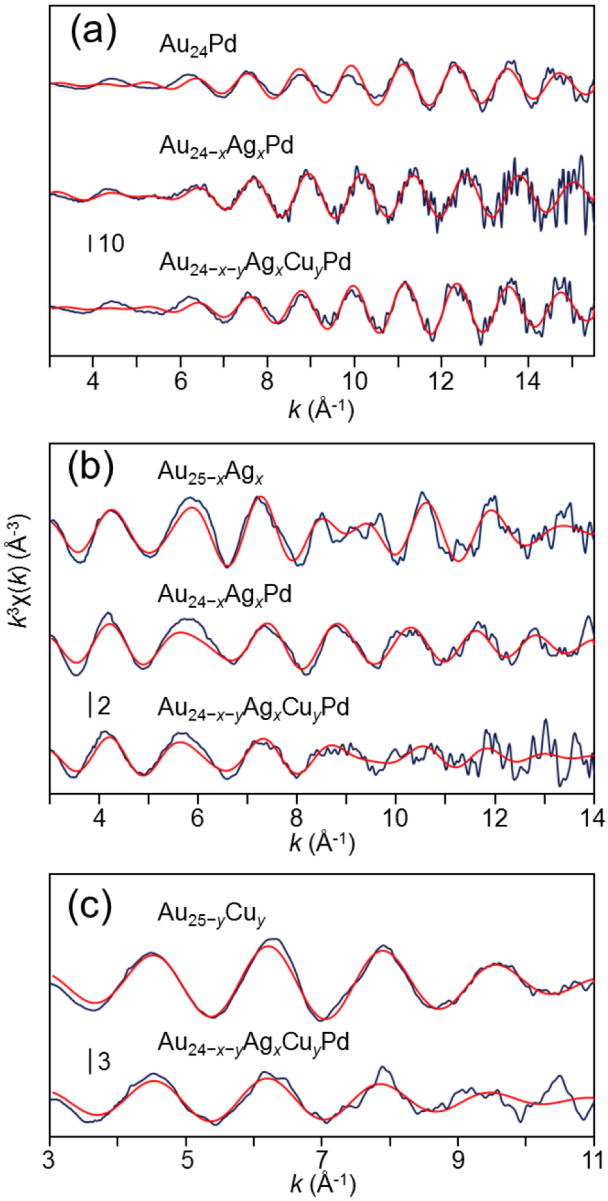

Fig. S9 (a) Experimental Pd K-edge EXAFS oscillations for $Au_{24}Pd(SC_{12}H_{25})_{18}$, $Au_{24-x}Ag_xPd(SC_{12}H_{25})_{18}$, and $Au_{24-x-y}Ag_xCu_yPd(SC_{12}H_{25})_{18}$. (b) Experimental Ag K-edge EXAFS oscillations for $Au_{24-x}Ag_xPd(SC_{12}H_{25})_{18}$ and $Au_{24-x-y}Ag_xCu_yPd(SC_{12}H_{25})_{18}$. (c) Experimental Cu K-edge EXAFS oscillations for $Au_{24-x-y}Ag_xCu_yPd(SC_{12}H_{25})_{18}$. The mass distributions of $Au_{24-x}Ag_xPd(SC_{12}H_{25})_{18}$ and $Au_{24-x-y}Ag_xCu_yPd(SC_{12}H_{25})_{18}$ used in these measurements are shown in Fig. S7 and S8, respectively.

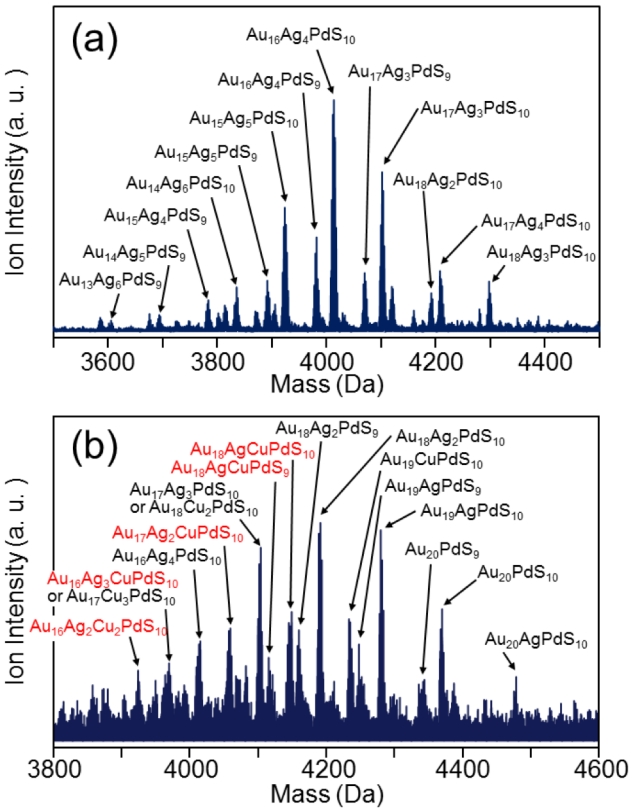

Fig. S10 Negative-ion MALDI mass spectrum of (a) $Au_{24-x}Ag_xPd(SC_{12}H_{25})_{18}$ (bottom of Fig. 2(a)) and (b) $Au_{24-x-y}Ag_xCu_yPd(SC_{12}H_{25})_{18}$ (bottom of Fig. 2(b)) observed with a laser fluence slightly higher than that used to observe non-destructive mass spectra. The appearance of fragments ions of $Au_zAg_xCu_yPdS_w$ ($x + y + z$ = 19–22; w = 9, 10) strongly indicates that Pd is substituted at the C site even in these samples.[16]

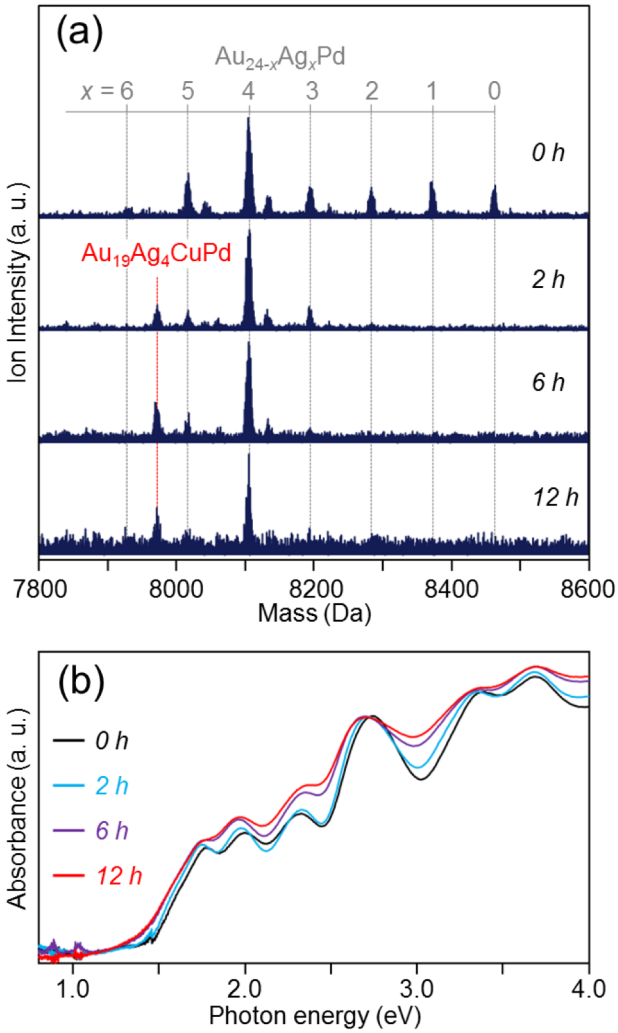

Fig. S11 (a) Negative-ion MALDI mass spectra and (b) optical absorption spectra of the products obtained by the reaction between $Au_{24-x}Ag_xPd(SC_{12}H_{25})_{18}$ and Cu-$SC_{12}H_{25}$. $Au_{24-x}Ag_xPd(SC_{12}H_{25})_{18}$ containing a different number of Ag atoms from that in Fig. 2(b) was used in this experiment.

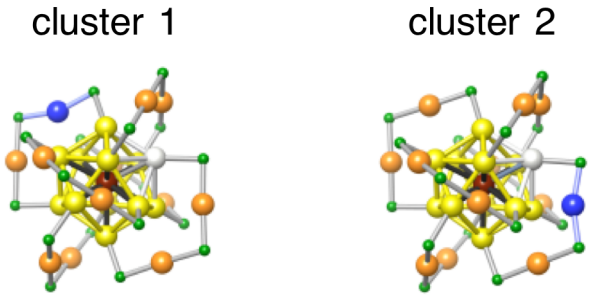

Fig. S12 Optimized structure for $[Au_{22}AgCuPd(SCH_3)_{18}]^0$ in which Pd, Ag and Cu are substituted at C, E and S sites, respectively. Because cluster 1 is more energetically stable than cluster 2 by 0.072 eV, the optical absorbance spectrum of $[Au_{22}AgCuPd(SCH_3)_{18}]^0$ (Fig. 5(b)) was calculated for cluster 1.

4. References

1. Y. Negishi, W. Kurashige, Y. Niihori, T. Iwasa and K. Nobusada, *Phys. Chem. Chem. Phys.*, 2010, **12**, 6219.
2. S. Wang, Y. Song, S. Jin, X. Liu, J. Zhang, Y. Pei, X. Meng, M. Chen, P. Li and M. Zhu, *J. Am. Chem. Soc.*, 2015, **137**, 4018.
3. S. Yang, S. Wang, S. Jin, S. Chen, H. Sheng and M. Zhu, *Nanoscale*, 2015, **7**, 10005.
4. A. Dass, A. Stevenson, G. R. Dubay, J. B. Tracy and R. W. Murray, *J. Am. Chem. Soc.*, 2008, **130,** 594.
5. S. Yamazoe, S. Takano, W. Kurashige, T. Yokoyama, K. Nitta, Y. Negishi and T. Tsukuda, *Nat. Commun*., 2016, **7**, 10414.
6. *TURBOMOLE*, version 6.3, TURBOMOLE GmbH, Karlsruhe, Germany.
7. C. Lee, W. Yang and R. G. Parr, *Phys. Rev. B: Condens. Matter*., 1988, 37, 785.
8. A. D. Becke, *J. Chem. Phys.*, 1993, **98**, 5648.
9. D. Andrae, U. Häußermann, M. Dolg, H. Stoll and H. Preuß, *Theor. Chim. Acta*, 1990, **77**, 123–141.
10. M. E. Casida in *Recent Advances in Density Functional Methods Part I*, ed. D. P. Chong, World Scientific, Singapore, 1995, vol. 1, pp. 155.
11. R. Bauernschmitt and R. Ahlrichs, *Chem. Phys. Lett.*, 1996, **256**, 454.
12. R. Bauernschmitt, M. Häser, O. Treutler and R. Ahlrichs, Chem. Phys. Lett., 1997, **264**, 573.
13. Y. Niihori, Y. Kikuchi, A. Kato, M. Matsuzaki and Y. Negishi, *ACS Nano*, 2015, 9, 9347–9356.
14. H. Qian, E. Barry, Y. Zhu and R. Jin, *Acta Phys.–Chim. Sin.*, 2011, 27, 513–519.
15. E. Gottlieb, H. Qian and R. Jin, *Chem.–Eur. J.*, 2013, 19, 4238–4243.
16. S. Sharma, W. Kurashige, K. Nobusada and Y. Negishi, *Nanoscale*, 2015, **7**, 10606.